ACSNANO

www.acsnano.org

ARTICLE

Aggregation of Heterogeneously Charged Colloids

Joshua M. Dempster[†] and Monica Olvera de la Cruz[*,†,‡]

[†]Department of Physics & Astronomy and [‡]Department of Materials Science and Engineering, Northwestern University, Evanston, Illinois 60208, United States

ABSTRACT: **Patchy colloids are attractive as programmable building blocks for metamaterials. Inverse patchy colloids, in which a charged surface is decorated with patches of the opposite charge, are additionally noteworthy as models for heterogeneously charged biological materials such as proteins. We study the phases and aggregation behavior of a single charged patch in an oppositely charged colloid with a single-site model. This single-patch inverse patchy colloid model shows a large number of phases when varying patch size. For large patch sizes we find ferroelectric crystals, while small patch sizes produce cross-linked gels. Intermediate values produce monodisperse clusters and unusual worm structures that preserve finite ratios of area to volume. The polarization observed at large patch sizes is robust under extreme disorder in patch size and shape. We examine phase-temperature dependence and coexistence curves and find that large patch sizes produce polarized liquids, in contrast to mean-field predictions. Finally, we introduce small numbers of unpatched charged colloids. These can either suppress or encourage aggregation depending on their concentration and the size of the patches on the patched colloids. These effects can be exploited to control aggregation and to measure effective patch size.**

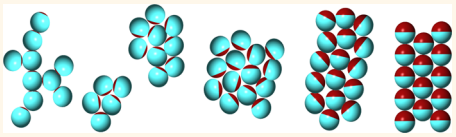

KEYWORDS: *patchy colloids, nanoparticles, ferroelectrical materials, self-assembly, colloid models*

Inspired by the anisotropic interactions of biology, colloidal science is increasingly focused on asymmetries in particle design. Breaking spherical symmetry unlocks diverse new options for self-assembling nanostructures.[1] Of particular interest are patchy colloids, whose surfaces are coated with materials of different properties. Most work in this area focuses on essentially inert or repulsive colloidal surfaces decorated with self-attracting patches. Common examples are hydrophobic patches[2] or colloids partly decorated with self-complementary DNA strands.[3] Researchers have predicted structures including wrinkled sheets,[4] tubes, and lamellae.[5] Still more elaborate structures such as Kagome lattices have been self-assembled by increasing the number of patches.[6]

Although these sorts of self-attracting particles have drawn the bulk of research efforts, other types of patchy interactions are possible. One significant example is the so-called inverse patchy colloid (IPC),[7] a colloid in which patches are attracted to the unpatched surfaces, while patch−patch and body−body interactions are neutral or soft repulsive. Neutral body−body and patch−patch interactions correspond to primitive models of associative fluids.[8,9] Soft repulsive body−body and patch−patch interactions model colloids with heterogeneous surface charge. Three experimental systems have realized these interactions in artificial colloids using DNA[10] and ionic double layers.[11,12] Understanding the role of heterogeneous charge patches is important for exploiting these new material design options but also for studying proteins. Proteins often carry heterogeneous surface charge,[13] which is the primary driver of aggregation behavior under the right conditions.[14] The anisotropy of protein interactions is essential for understanding aggregation behavior,[15,16] and general, high-fidelity coarse-grain models of proteins therefore need to account for charged as well as hydrophobic patches. Controlling protein aggregation is critical in the food[17] and pharmaceutical[18] industries and for understanding neurodegenerative diseases such as Alzheimers.[19]

Motivated in part by these considerations, extensive work has been done for particles with two like patches at opposing poles.[20−24] Here we study the phases of *single*-patch IPCs in detail and uncover a rich set of discrete phases. We introduce a modified Kern−Frenkel potential and find it replicates the polarized clusters found in much finer grain simulations. We study the phase diagram first at low temperatures and determine the cold phases as a function of patch size. Next, we examine the survival of polarization in the face of disorder and confirm that it is robust. We then move from the low-temperature regime to consider the temperature dependence of the phase diagram. We construct liquid−vapor coexistence curves for those patch sizes that phase-segregate and confirm the existence of a polarized liquid phase, in contradiction to mean-field predictions. Finally, we introduce charged, unpatched colloids and examine their effects on aggregation. The results can be exploited to inhibit or encourage colloid

Received: February 17, 2016
Accepted: June 2, 2016
Published: June 2, 2016

DOI: 10.1021/acsnano.6b01218
ACS Nano 2016, 10, 5909−5915

aggregation and to make sensitive measurements of colloid patch size.

RESULTS AND DISCUSSION

Model. The Kern−Frenkel potential has been used extensively to study patchy colloids.[25] It operates by examining a single point on each of two interacting spheres, specifically the points intersected by a line connecting the sphere centers.[26] If both points are of the attractive material, the model applies a radial attractive potential. A similar model for IPCs is found by adopting a potential of the form

$$U(\mathbf{r}, \boldsymbol{\omega}) = U_R(r) + \alpha(\mathbf{r}, \boldsymbol{\omega})U_E(r) \quad (1)$$

Here, U_R is the purely repulsive hard sphere potential, U_E is the Debye−Hückel electrostatic interaction between uniformly (equally) charged spheres, $\mathbf{r}$ is the vector between spheres, and $\boldsymbol{\omega}$ contains the orientation of each sphere. U_E is taken as always positive, while $\alpha \in [-1,1]$ carries the sign of the interaction. To improve equilibration rates, we use a slightly softened hard-sphere interaction of the form

$$U_R(r) = \begin{cases} \psi\left(\left(\frac{\sigma}{r}\right)^{12} - 1\right) & r < \sigma \\ 0 & r \geq \sigma \end{cases} \quad (2)$$

where ψ is an energy in thermal units and σ is the particle diameter. U_E is drawn from the potential between two identical charged spherical surfaces when the screening length λ is less than the diameter[27]

$$U_E(r) = \begin{cases} \psi \exp\left(-\frac{r-\sigma}{\lambda}\right) & r - \sigma \leq 5\lambda \\ 0 & r - \sigma > 5\lambda \end{cases} \quad (3)$$

where we truncated the potential at 5λ. Opposite charge densities are assumed for the patched and unpatched portions. This choice for radial potential is logical given the two assumptions that the radial dependence is separable and that the patch boundary has no effect on points far from the boundary. However, any positive radial potential with the same range is likely to produce similar aggregates.

For the case of particles with a single, circular patch, we define colloid orientation in terms of a normalized vector $\mathbf{v}$ that points from the colloid center to the center of the patch (Figure 1). With axial symmetry and fixed charge surface charge

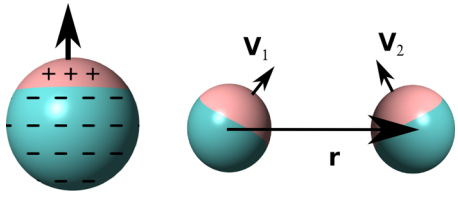

Figure 1. One-patch inverse patchy colloids. The vectors $\mathbf{v}_1$, $\mathbf{v}_2$, and $\mathbf{r}$ contain the necessary information for the pairwise potential.

distributions, α reduces to a function of three variables: $\nu_1 = \mathbf{v}_1 \cdot \hat{\mathbf{r}}$, $\nu_2 = \mathbf{v}_2 \cdot \hat{\mathbf{r}}$, and $\nu_3 = \mathbf{v}_1 \cdot \mathbf{v}_2$. Since a Kern−Frenkel model only tests the two closest points on the spheres, only the variables ν_1 and ν_2 are needed. Additionally, the system must be invariant under simultaneous exchange of indices and reversal of $\mathbf{r}$. These restrictions motivate functions of the form

$$\alpha(\nu_1, \nu_2) = q_1(\nu_1)q_2(-\nu_2) \quad (4)$$

The q functions describe effective charge densities at the points selected by ν_1 and $-\nu_2$. In principal, these may involve averaging over the physical charge distributions at some distance around the two points to yield smooth functions; however, this paper will consider only the simplest case of a square well in ν_1 and ν_2, as in the original Kern−Frenkel model. If the opening angle of patch i is θ_i, then the square well takes the form

$$\alpha(\nu_1, \nu_2) = \mathrm{sgn}(\nu_1 - \cos\theta_1)\mathrm{sgn}(-\nu_2 - \cos\theta_2) \quad (5)$$

Equation 5 only closely approximates the real orientational dependence in the limit of extremely short screening length λ. Accordingly, we choose $\lambda = 0.08\ \sigma$ for this work. More sophisticated q functions could better capture finite screening length effects. Nonetheless, the adapted Kern−Frenkel model of eqs 1−5 successfully reproduces the counterintuitive ferroelectric phase found from more elaborate models,[11] as shown below. In addition, it has the virtues of computational speed and clear exhibition of the role of orientational energy degeneracy in particle aggregates. In contrast, the multisite and spherical harmonic models used by Stipsitz and co-workers for two-patch particles[28] may be more useful for multipatch models or longer screening lengths.

IPC Cold Phases. We simulate the aggregation of IPCs for various values of the opening angle θ using NVT Monte Carlo, as illustrated in Figure 2. The aggregate phases differ from either ordinary patchy particles or dipoles. For spheres evenly divided into two charge phases, we reproduced the polarized aggregates first found by Hong and co-workers[11] and extend their results to find the close-packed crystalline ground state. The result is a macroscopically polarized aggregate displaying colloidal ferroelectricity (Figure 2b, first panel). Between θ = 1.5 and θ = 1.4, a transition occurs in which aggregates are locally polarized and extensive with system size but prefer a larger surface area (Figure 2b, second panel). Between θ = 1.3 and θ = 1.2, aggregates are limited to finite sizes, and their surfaces are coated with the excess charge phase. These aggregates reach a maximum size even under very slow annealing (Figure 2b, third panel). As the patch area shrinks further, the coordination number for colloids falls. Aggregates turn into clumpy gels that become increasingly open, leading to a cross-linked gel in the limit of very small patch sizes (Figure 2b, final panel).

The aggregate phases derive from the symmetries of close-packed spheres. The maximum coordination number for the IPC fluids is twice the number of particles that can be fit on a patch. Specifically, to form extended compact bodies, colloids must fit six contacts on each of their two surface types. The minimum opening angle that allows six neighbors on the patch is 1.249 for HCP and 1.294 for FCC structures. As the opening angle approaches θ = 1.3, maintaining polarization, defined as $P \equiv 1/n\ \|\sum_i \mathbf{v}_i\|$, becomes more entropically expensive (Figure 3a). Enthalpy produces a cylindrical core polarized along its axis (Figure 3b). However, entropy limits the diameter of the core through a disinclination which rotates colloids so their patches face inward (Figure 3c). The result is thick wormlike structures with fluctuating thickness (Figure 3d). Where ordinary liquids minimize their surface, the disinclined liquid conserves its surface at a fixed ratio to its volume.

At θ < 1.25, no close-packed structure can avoid repulsive contacts. The effective valence of the colloids is now less than 12. Studies of other low-valence systems have produced

DOI: 10.1021/acsnano.6b01218
ACS Nano 2016, 10, 5909−5915

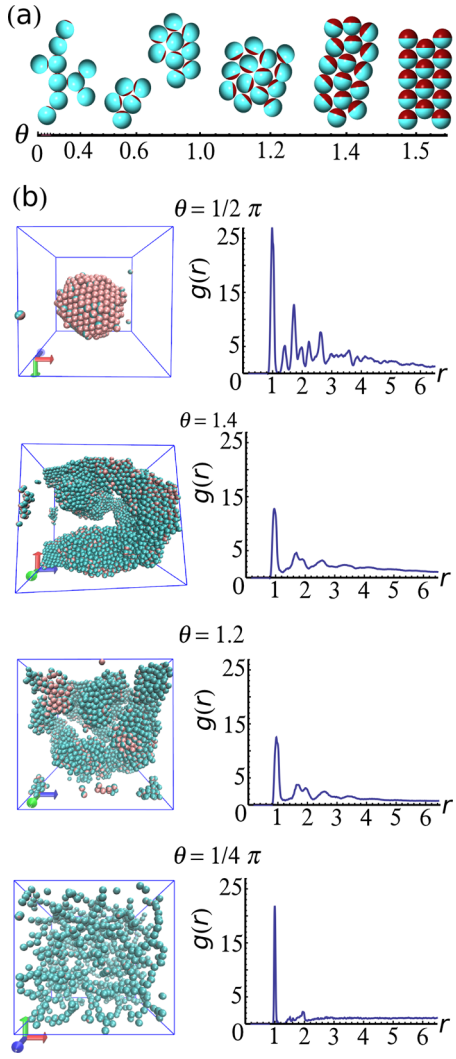

Figure 2. Overview of annealed cold phases of the modified Kern–Frenkel model for varying patch sizes. (a) Primitive figure showing the transition from cross-linked gels at very small patch sizes to polarized crystals at $\theta \geq 1.5$. (b) Details at four specific values of θ using NVT simulations. Distinct phases are the polarized close-packed crystal (θ = 1.57, ψ-normalized temperature T^* = 0.3125, density ρ^* = 0.286(σ^{-3})), a wormlike glass with extended surface (θ = 1.4, T^* = 0.3125, ρ^* = 0.477), size-limited isotropic clusters (θ = 1.2, T^* = 0.303, ρ^* = 0.382), and cross-linked gels (θ = 0.39, T^* = 0.025, ρ^* = 0.191). For the cases of θ = 1.2 and θ = 1.4, we removed gas-phase colloids for visual clarity.

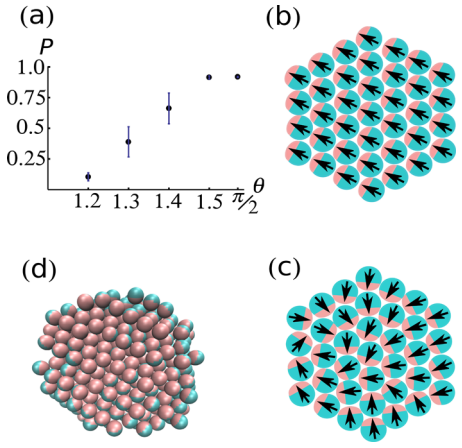

Figure 3. Geometry and polarization of the condensed phases. (a) Polarization as a function of opening angle size for systems annealed to T^* = 0.333. Gibbs ensemble Monte Carlo was used to obtain contiguous condensed phases. Bars show the variance of five samples. Sample sizes ranged from 200 to 1000 particles depending on how many were found in the denser phase. (b) Polarized close-packed phase in 2D. (c) Smaller patch sizes produce a vortex-like disinclination that reorients colloids at the fringes so their patches face the center, limiting growth. (d) At θ = 1.4, the condensed phase has a polarized core with the ordering of (b), surrounded by a sheath of inward-oriented colloids similar to (c). This results in long worms with finite diameter. The cross section of such a worm is shown here.

divergent results. For particles with a fixed number of independent binding sites on their surfaces, low-valence regimes produce a condensed phase of cross-linked gels or "empty fluids," as described by Wertheim theory.[29] On the other hand, for ordinary Janus colloids, low-valence/small-patch regimes lead to micellization.[30] We find that IPCs with $\theta \in [0.6, 1.25]$ form finite clusters, but these clusters are often larger than true micelles (Figure 4). The finite radii of the clusters are determined by patch geometry. If the surface of a cluster is a flat plane (infinite radius), then for patch sizes less than the critical angle it is impossible for new colloids to adsorb to the cluster without making unfavorable body–body contacts. Thus, some non-zero curvature is necessary to make adsorption favorable, and cluster growth halts once curvature reaches this limit.

As patch sizes shrink further the clusters become extended and transition into cross-linked gels. Because patches can bind anywhere on the unpatched surface, IPCs with small patches resemble particles with independent, movable binding sites. Aside from binding site mobility, this is similar to the situation described by Wertheim theory and produces similar gels at low temperatures. It may also be compared to the saturated square-well model, which again produces ideal gels.[31]

In the limit of low temperature and very small patch sizes, it is straightforward to characterize the gels analytically. At low temperatures,the number of bonds is equal to the number of patches (note that this is not equivalent to saying that each particle has a single bond). Consequently, all configurations have equal enthalpy and the free energy is entirely determined by entropy. The entropy for each bound colloid is the log of the free surface area of the colloid it is bound to; *i.e.*, the area the bound colloid can explore without colliding with another colloid. The free surface for a chain terminus (colloid with only one neighbor) is the surface of a sphere of radius σ with a hole centered on the neighbor due to repulsive interactions between the bodies of the existing neighbor and any new neighbor. The size of the hole can be determined trigonometrically. The resulting free area is $\pi\ (3 - 2\lambda - \lambda^2)$ in σ-normalized units, where λ is the effective range of electrostatic repulsion. The free surface for a midchain colloid (colloid with two neighbors) is $2\pi(1 - 2\lambda - \lambda^2)$ if the chain is not sharply kinked, *i.e.*, the area of a sphere with two holes. The free surface is 10% greater in the maximally kinked case, where the bead and its neighbors form an equilateral triangle. We approximate the thermodynamic mean of the free surface with the free surface of the straight line configuration of the three beads.

Consider the case that a contiguous network of N colloids has n terminal strands. The equilibrium condition is that the

DOI: 10.1021/acsnano.6b01218
ACS Nano 2016, 10, 5909–5915

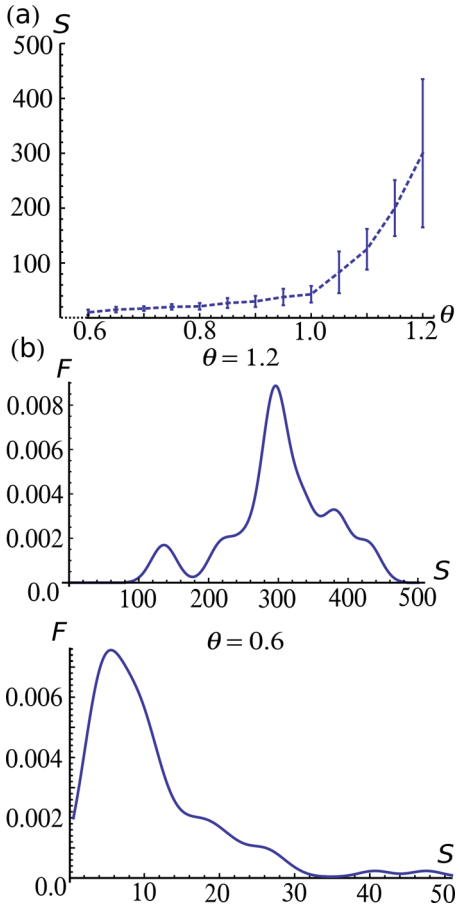

Figure 4. Annealed cluster size. (a) Mean cluster size S for clusters with three or more colloids for different patch sizes. Bars show standard deviations. Cluster sizes diverge as the opening angles approach the critical angle $\theta = 1.25$ where close-packing becomes possible. S is obtained by NVT simulations at density $\rho^* = 0.191\sigma^{-3}$. Final temperatures varied from $T^* = 0.303$ to $T^* = 0.174$ and system size from 4000 to 1000, with lower temperatures and smaller systems for smaller patch sizes. (b) Smoothed histograms of cluster size for $\theta = 1.2$ and $\theta = 0.6$.

total free surface of the terminal and midstrand colloids be equal, or

$$n(3 - 2\lambda - \lambda^2) = 2(N - 2n)(1 - 2\lambda - \lambda^2) \quad (6)$$

yielding the branching probability $n/N = 0.270$ for $\lambda = 0.08$. In obtaining this result, we ignored hard-sphere interactions for colloids more than two steps removed in the network. We also discarded the much rarer cases of colloids that have more than three neighbors and treated the body−body electrostatic potential as an infinite repulsion cut at $(1 + \lambda)\sigma$. Despite the crudeness of this estimate, we find excellent agreement with NVT simulations ($n/N = 0.268 \pm 0.003$). The simulation result is insensitive to patch size for the values we examined ($0.2 <= \theta <= 0.4$) and was obtained for the annealed system. For a hard-quenched system, branching drops slightly to 0.25 ± 0.014.

Effects of Disorder on Polarization. From the previous discussion, it is clear that polarization is both critical for unbounded aggregation and sensitive to patch size. The disorder present in real physical systems could plausibly disrupt the polarized phase. Therefore, we examine polarization in nonuniform systems. One common form of disorder in a manufacturing or biological process is a noncircular patch edge. Consider colloids with patch boundaries given by

$$\theta(\phi) = \frac{\pi}{2}\left(1 + \frac{1}{2}\tanh\left(a\sum_{n=1}^{N}\frac{\xi_n}{n}\cos(n\phi + \pi\zeta_n)\right)\right) \quad (7)$$

where θ is the lattitude of the boundary, ϕ is the azimuthal angle on the sphere, a is a free parameter, and the ξ_n, ζ_n are random numbers chosen uniformly in the interval $[-1,1]$. We exclude the $n = 0$ node, so the total area of the patch is one-half the sphere area. This form is chosen to guarantee convergence for the variance of the argument of tanh while allowing the length of the boundary to diverge.

We study irregular patches using a fine-grain system that models colloid surfaces with 5000 point charges, similar to the model used by Hong and co-workers.[11] The point charges interact *via* the Debye−Hückel potential and a purely repulsive shifted Lennard-Jones potential. HOOMD-Blue simulates the Brownian dynamics.[33−36] Due to the large number of particles per colloid and divergent length scales, only small systems can be studied. Nonetheless, we observe the same polarized glass phase with the most extreme patch shape disorder attempted ($a = 2$, $N = 200$). Since such clusters can easily aggregate by connecting positive with negative faces, this result suggests that polarized clusters can grow to arbitrary size. Figure 5a illustrates a typical observed configuration.

The other probable form of patch disorder is polydispersity in patch size. Rather than a single opening angle for all colloids, we choose angles for each colloid uniformly in the interval $[\pi/2 - b, \pi/2 + b]$. The single-site model shows that polarization survives disorder up to about $b = 0.8$. At this level of disorder the variance in total charge on each colloid is $\pm 0.577Q_0$, where

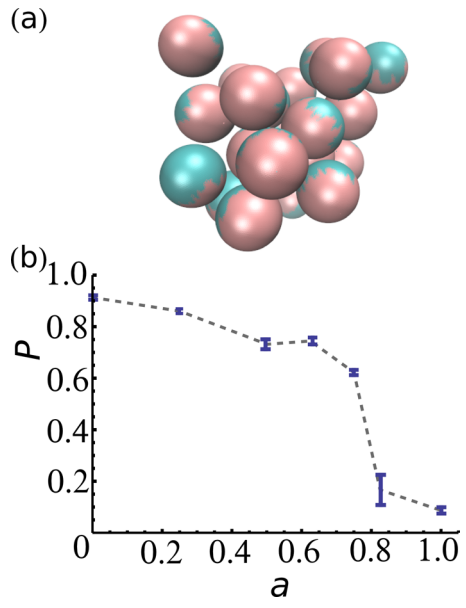

Figure 5. Robustness of polarization in condensates of polydisperse colloids. (a) Sample cluster formed for ragged patch boundaries when $\alpha = 2$. Despite highly irregular patch shapes, clusters display orientational ordering that produces a net polarization. Colloids are drawn with diameters slightly smaller than their hard-sphere contact distances. (b) Polarization in the solid phase when patch sizes are polydisperse, with opening angles varying uniformly by a from $1/2\,\theta$. Polarization is again quite robust, failing only at around $a = 0.8$ radians. The solid phases have 700−900 particles.

DOI: 10.1021/acsnano.6b01218
ACS Nano 2016, 10, 5909−5915

Q_0 is the charge on a colloid with no patch. Figure 5b plots the polarization in the condensed phase at $T^* = 0.33$ for various values of b.

These results together show great robustness in the polarization of condensed phases. Polarization survives polydispersity far in excess of probable synthesis defects or thermal variations between identically folded proteins. Consequently, large, high-density single-patch IPC aggregates should display ferroelectric behavior.

Vapor–Condensate Coexistence. We return to monodisperse colloids and examine liquid–vapor coexistence curves using the single-site model. We use Gibbs ensemble Monte Carlo (GEMC) in all cases. Figure 6 summarizes the results.

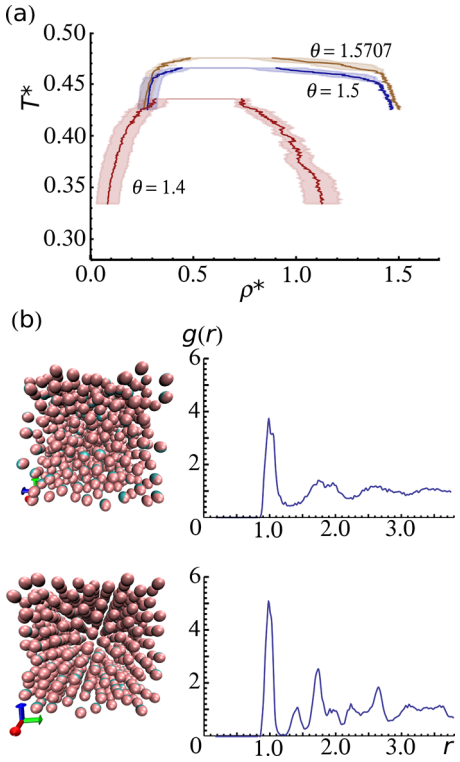

Figure 6. Gibbs ensemble results for phase separation. (a) Vapor/condensate coexistence in single-component systems. Shaded regions show uncertainties. Due to the extremely short range of the potential, the GEMC algorithm is unable to move sufficient particles from the gas phase to the densely packed condensed phase at $\theta = 1.57$ and $\theta = 1.5$. Thus, it overestimates gas phase density. Simulations performed with lower initial densities suggest the true gas densities are less than 0.1 unless very close to the critical temperature. This problem does not arise for $\theta = 1.4$, since the condensed phase always includes voids for gas colloids to move into. We did not observe any phase segregation for $\theta = 1.3$ or $\theta = 1.2$. (b) Examples of the liquid ($T^* = 0.46$, $\rho^* = 0.81$) and solid ($T^* = 0.43$, $\rho^* = 1.47$) phases for $\theta = 1.57$. All observed liquids for $\theta > 1.4$ were polarized. Polarization in the 1−0−0 and 1−1−1 directions occurs with roughly equal frequency. Colloids are rendered with reduced diameters to show lattice structure.

For neutral and nearly neutral charge ($\theta = 1.57$, $\theta = 1.5$), we find an abrupt phase transition with estimated critical points at $T^* = 0.48$, $\rho^* = 0.7$ and $T^* = 0.47$, $\rho^* = 0.7$. Here, T^* is the inverse of ψ and ρ^* is the density in volume units of σ^3. For $\theta = 1.4$ the critical temperature drops slightly to 0.44 and phase separation is more gradual. The liquid phase here includes large, contiguous voids to provide surfaces for the disinclinations described earlier. Phase separation is geometrically possible for $\theta = 1.3$, but we did not observe it *via* annealing. This is consistent with our entropic analysis earlier: as θ approaches the minimum necessary to fit six particles on a patch in a close-packed crystal, the critical temperature for the polarized crystal approaches zero and this phase becomes kinetically inaccessible. Confining orientation, as by a strong external field, may reduce the minimum patch size needed for segregation.

In this work, we focus on colloid aggregation out of solution. We leave the colloidal liquid–solid boundaries for future work. However, we can address the question of whether the liquid state preceding aggregate solidification is polarized. Eggen and van Roij used the linearized Poisson–Boltzmann ion distribution and a cell model with mean-field positioning to predict that heterogeneously charged particles would not display orientational ordering without positional ordering.[32] By contrast, Hong and co-workers found polarization in small glassy clusters with positional disorder.[11] By examining the liquid states at temperatures slightly below the critical point, we confirmed that the liquid states are polarized as well. The onset of polarization is concurrent with phase segregation for all cases. This suggests that caution should be used with mean-field methods for heterogeneously charged spheres when screening lengths are small compared to diameters.

Effects of Uniformly Charged Colloids on Vapor–Condensate Coexistence. Aggregation for small patch sizes is limited by the need to avoid patch–patch and body–body contacts. Including uniformly charged no-patch colloids (NPCs) with the same charge sign as the patch on the IPCs provides an alternate mechanism for making all contacts energy-negative. In principal this should make aggregation possible for patch angles below 1.3. We re-examine phase separation with various percentages of the IPCs replaced with NPCs, with results shown in Figure 7. We label the relative concentration of NPCs in the unseparated (high-temperature) phase x. Table 1 summarizes the ratio of NPCs to IPCs in the condensed phases for three values of patch opening. Values less than x indicate that the solid expels NPCs and corresponds to NPC-inhibited aggregation, while values greater than x correspond to NPC-assisted aggregation.

NPCs in a $\theta = 1.57$ system have little effect for small concentrations as they are expelled to the gas phase (Figure 7 top). However, when $x = 0.2$, the presence of NPCs in the condensed phase increases by 1 order of magnitude. The critical temperature is lowered and phase segregation slowed while the low-temperature density is reduced. We conclude that the NPCs are forcing contacts between like charges in the solid phase.

In contrast, even very small numbers of NPCs ($x = 0.025$) dramatically alter the condensed phases for $\theta = 1.4$ (Figure 7 middle). The resulting condensates show lower polarization than the single-component liquid crystal formed with $\theta = 1.57$ but comparable densities. At $x = 0.1$ polarization in the condensed phase drops sharply, and at $x = 0.2$ the critical temperature is suppressed.

For $\theta = 1.2$, phase segregation becomes possible for $0.05 < x \leq 0.1$ (Figure 7 bottom). The relatively high concentration necessary for phase separation with $\theta = 1.2$ *vs* $\theta = 1.4$ reflects the different mechanisms operating in each case. For $\theta = 1.4$, aggregation is controlled by entropy and is easily influenced by small net charge differences. For $\theta = 1.2$, simple geometry limits aggregation. Thus, phase separation at $\theta = 1.2$ is only possible

DOI: 10.1021/acsnano.6b01218
ACS Nano 2016, 10, 5909–5915

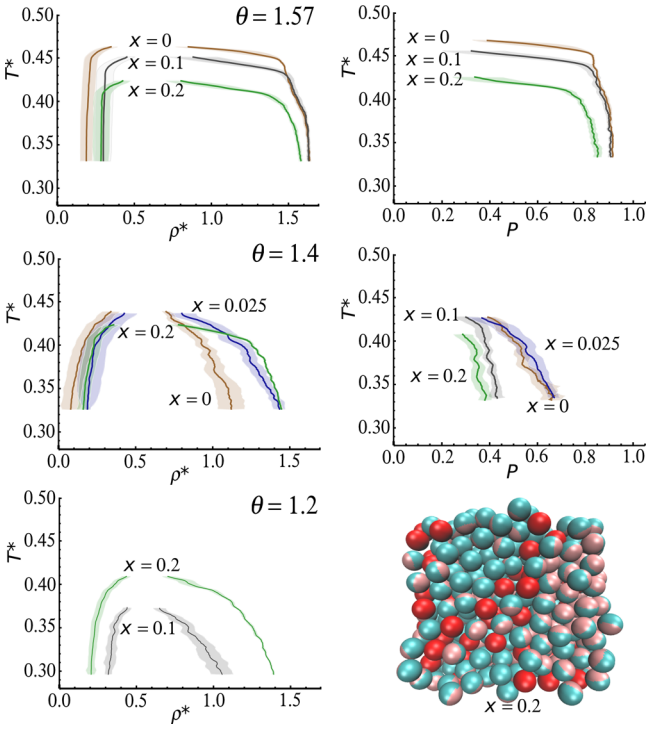

Figure 7. Effects of introducing NPCs on phase coexistence. The initial (unseparated) ratio of NPCs to total colloids is given by x. Densities (left) are evaluated for the combined NPC/IPC colloids; see Table 1 for final fractional concentration of NPCs in the solid phases. Condensate polarizations (right) are calculated from the IPCs alone. Polarization curves are truncated at the level where net polarization becomes indistinguishable from random fluctuations (determined by comparison with the gas phase). For θ = 1.2, no polarization is observed. A typical example of the solid state is shown instead, with NPCs drawn in dark red.

with enough NPCs to provide an NPC neighbor for each IPC. The result is a glassy structure that displays no net polarization.

These effects are potentially useful for controlling aggregation but also for probing experimental systems in which the opening angle may not be known and competing potentials may either drive or hinder aggregation.

Conclusion. Heterogeneously charged colloids are interesting both as potential liquid-state materials and as models for proteins. For particles with a single patch of charge opposite to the rest of the particle, we find that varying the patch size produces phases including a liquid crystal, worms of finite surface area, size-limited clusters, and colloidal gels. The polarized liquid/solid phases are notably robust to extreme polydispersity in patch characteristics. Phase diagrams can be modulated by introducing unpatched charged colloids.

Many significant questions remain to be explored. Among these are the role of screening length in the phase diagram and whether the generalization of the model suggested after eq 4 can capture longer screening lengths; assembly with multiple patches; and the effects of external fields. For example, an electric field could be used to break the cross-links in the gel phase observed for small patch sizes, effectively switching between a gel and an electrorheological fluid. It would also be interesting to study a very large system in the worm phase (patch sizes $\theta \in (1.3, 1.5)$). Current work suggests that the worms cross-link, forming a "supergel" in which each worm acts as a polymer. These and other potential applications are fertile ground for future work.

MATERIALS AND METHODS

The four annealed phases for IPCs shown in Figure 2 are found using multiple runs of NVT MC with parameters quoted in the caption. Particle counts begin at 1000 but include runs up to 8000 for θ = 1.2 and θ = 1.4 to check whether clusters were extensive with system size. To produce clear figures, gas-state colloids were removed by recursively eliminating particles with fewer than three neighbors.

The polarization data given in Figure 3 is obtained by annealing the Gibbs ensemble Monte Carlo (GEMC) from T^* = 0.5 to T^* = 0.303 over 10000 Brownian timesteps (the time required to diffuse a colloid by its diameter). The initial densities are ρ^* = 0.55. No preference for any particular patch size is observed in the condensates.

Figure 3 is generated by NVT simulations at density ρ^* = 0.191. We also examined densities of ρ^* = 0.382 with no significant changes to cluster size observed. Final temperatures vary from T^* = 0.303 to T^* = 0.174 as needed to achieve solidification of the clusters, with lower temperatures for smaller patch/cluster sizes.

The branching probability for the gel phases is tested using triplets of 1000-colloid NVT runs and annealing from T^* = 0.2 to T^* = 0.1 over 4000 Brownian timesteps with density ρ^* = 0.192. We test the quenched connectivity with constant temperature T^* = 0.02.

Irregular patch shape simulations use 27 colloids composed of 5058 particles spaced uniformly and rigidly over the colloid surface. Particles interact *via* the purely repulsive shifted Lennard-Jones potential with a cutoff $r_c = 1.12\sigma_p$, where σ_p is the LJ diameter for each particle. The diameter σ_p is chosen to be 0.025σ or 1.5× the spacing between particles. Particles also interact through the screened Coulomb potential $\epsilon r^{-1} \exp -r/\lambda$, where $\epsilon = \pm 0.01$. As in all cases examined in this paper, $\lambda = 0.08\sigma$ and the electrostatic potential was cut at 5λ.

Liquid−vapor coexistence curves and polarization values are found using five runs of 1000-particle GEMC per parameter for both the single- and two-component systems. Although Maxwell reconstruction is also a popular method, the Gibbs ensemble has the advantage of determining the liquid−vapor phase boundary in a single simulation and is commonly used for patchy colloids.[15,26,30] Its chief disadvantage is its difficulty describing coexistence between more than two phases. However, our main concern in this section is the onset of aggregation, whether liquid or solid. GEMC is a natural choice for determining this boundary. Uncertainties are given by the variance between runs. Coexistence curves use an initial density ρ^* = 0.55. Annealing rates vary by patch size and are determined by observing equilibration times for fixed-temperature simulations at temperatures ranging from T^* = 0.45 to T^* = 0.33.

All simulations use cubic periodic boundary conditions.

AUTHOR INFORMATION

Corresponding Author

*E-mail: m-olvera@northwestern.edu.

Notes

The authors declare no competing financial interest.

Table 1. Fractional Population of NPCs in Solid Phases

IPC patch angle	x = 0.025	x = 0.05	x = 0.1	x = 0.2
1.2			0.109 ± 0.006	0.206 ± 0.002
1.4	0.032 ± 0.005	0.0507 ± 0.0004	0.0970 ± 0.0007	0.141 ± 0.002
1.57	0	0.003 ± 0.001	0.002 ± 0.001	0.022 ± 0.003

DOI: 10.1021/acsnano.6b01218
ACS Nano 2016, 10, 5909−5915

ACKNOWLEDGMENTS

We thank V. Pryamitsin and M. Shen for helpful discussions. We acknowledge support from NSF Grant No. DMR-1309027. Simulations were performed on TARDIS, which is a computer cluster financially supported by the Air Force Office of Scientific Research (AFOSR) under Award No. FA9550-10-1-0167, and on the Quest High Performing Computer Cluster maintained by Northwestern University.

REFERENCES

(1) Zhang, J.; Luijten, E.; Granick, S. Toward Design Rules of Directional Janus Colloidal Assembly. *Annu. Rev. Phys. Chem.* **2015**, *66*, 581−600.
(2) Glaser, N.; Adams, D. J.; Böker, A.; Krausch, G. Janus Particles at Liquid-Liquid Interfaces. *Langmuir* **2006**, *22*, 5227−5229.
(3) Xing, H.; Wang, Z.; Xu, Z.; Wong, N. Y.; Xiang, Y.; Liu, G. L.; Lu, Y. DNA-Directed Assembly of Asymmetric Nanoclusters Using Janus Nanoparticles. *ACS Nano* **2012**, *6*, 802−809.
(4) Vissers, T.; Preisler, Z.; Smallenburg, F.; Dijkstra, M.; Sciortino, F. Predicting Crystals of Janus Colloids. *J. Chem. Phys.* **2013**, *138*, 164505.
(5) Preisler, Z.; Vissers, T.; Smallenburg, F.; Munaó, G.; Sciortino, F. Phase Diagram of One-Patch Colloids Forming Tubes and Lamellae. *J. Phys. Chem. B* **2013**, *117*, 9540−9547.
(6) Chen, Q.; Bae, S. C.; Granick, S. Directed Self-Assembly of a Colloidal Kagome Lattice. *Nature* **2011**, *469*, 381−384.
(7) Bianchi, E.; Blaak, R.; Likos, C. N. Patchy Colloids: State of the Art and Perspectives. *Phys. Chem. Chem. Phys.* **2011**, *13*, 6397−6410.
(8) Smith, W. R.; Nezbeda, I. A Simple Model for Associated Fluids. *J. Chem. Phys.* **1984**, *81*, 3694−3699.
(9) Wertheim, M. S. Integral Equation for the Smith-Nezbeda Model of Associated Fluids. *J. Chem. Phys.* **1988**, *88*, 1145−1155.
(10) Feng, L.; Dreyfus, R.; Sha, R.; Seeman, N. C.; Chaikin, P. M. DNA Patchy Particles. *Adv. Mater.* **2013**, *25*, 2779−2783.
(11) Hong, L.; Cacciuto, A.; Luijten, E.; Granick, S. Clusters of Charged Janus Spheres. *Nano Lett.* **2006**, *6*, 2510−2514.
(12) van Oostrum, P. D. J. l; Hejazifar, M.; Niedermayer, C.; Reimhult, E. Simple Methods for the Synthesis of Inverse Patchy Colloids. *J. Phys.: Condens. Matter* **2015**, *27*, 234105.
(13) Park, J. M.; Muhoberac, B. B.; Dubin, P. L.; Xia, J. Effects of Protein Charge Heterogeneity in Protein-Polyelectrolyte Complexation. *Macromolecules* **1992**, *25*, 290−295.
(14) Majhi, P. R.; Ganta, R. R.; Vanam, R. P.; Seyrek, E.; Giger, K.; Dubin, P. L. Electrostatically Driven Protein Aggregation: Beta-Lactoglobulin at Low Ionic Strength. *Langmuir* **2006**, *22*, 9150−9159.
(15) Liu, H.; Kumar, S. K.; Sciortino, F. Vapor-Liquid Coexistence of Patchy Models: Relevance to Protein Phase Behavior. *J. Chem. Phys.* **2007**, *127*, 084902.
(16) Quang, L. J.; Sandler, S. I.; Lenhoff, A. M. Anisotropic Contributions to Protein-Protein Interactions. *J. Chem. Theory Comput.* **2014**, *10*, 835−845.
(17) Ju, Z. Y.; Kilara, A. Effects of Preheating on Properties of Aggregates and of Cold-Set Gels of Whey Protein Isolate. *J. Agric. Food Chem.* **1998**, *46*, 3604−3608.
(18) Cromwell, M. E. M.; Hilario, E.; Jacobson, F. Protein Aggregation and Bioprocessing. *AAPS J.* **2006**, *8*, E572−E579.
(19) Ross, C. A.; Poirier, M. A. Protein Aggregation And Neurodegenerative Disease. *Nat. Med.* **2004**, *10*, S10−S17.
(20) Bianchi, E.; Kahl, G.; Likos, C. N. Inverse Patchy Colloids: From Microscopic Description to Mesoscopic Coarse-Graining. *Soft Matter* **2011**, *7*, 8313−8323.
(21) Bianchi, E.; Kahl, G.; Likos, C. N. Self-Assembly of Heterogeneously Charged Particles Under Confinement. *ACS Nano* **2013**, *7*, 4657−4667.
(22) Ferrari, S.; Bianchi, E.; Kalyuzhnyi, Y.; Kahl, G. Inverse Patchy Colloids with Small Patches: Fluid Structure and Dynamical Slowing Down. *J. Phys.: Condens. Matter* **2015**, *27*, 234104.
(23) Kalyuzhnyi, Y. V.; Vasilyev, O. A.; Cummings, P. T. Inverse Patchy Colloids with Two and Three Patches: Analytical and Numerical Study. *J. Chem. Phys.* **2015**, *143*, 044904.
(24) Noya, E. G.; Bianchi, E. Phase Behavior of Inverse Patchy Colloids: Effects of the Model Parameters. *J. Phys.: Condens. Matter* **2015**, *27*, 234103.
(25) Sciortino, F.; Giacometti, A.; Pastore, G. A Numerical Study of One-Patch Colloidal Particles: From Square-Well to Janus. *Phys. Chem. Chem. Phys.* **2010**, *12*, 11869.
(26) Kern, N.; Frenkel, D. Fluid-fluid Coexistence in Colloidal Systems with Short-Ranged Strongly Directional Attraction. *J. Chem. Phys.* **2003**, *118*, 9882.
(27) Verwey, E. J. W.; Overbeek, J. Th. G. *Theory of the Stability of Lyophobic Colloids*; Elsevier: New York, 1948.
(28) Stipsitz, M.; Kahl, G.; Bianchi, E. Generalized Inverse Patchy Colloidal Model. *J. Chem. Phys.* **2015**, *143*, 114905.
(29) Sciortino, F.; Zaccarelli, E. Reversible Gels of Patchy Particles. *Curr. Opin. Solid State Mater. Sci.* **2011**, *15*, 246−253.
(30) Sciortino, F.; Giacometti, A.; Pastore, G. Phase Diagram of Janus Particles. *Phys. Rev. Lett.* **2009**, *103*, 237801.
(31) Speedy, R. J. Models for Fluids and Crystals of Molecules with Valency. *J. Phys. Chem.* **1993**, *97*, 2723−2731.
(32) Eggen, E.; van Roij, R. Poisson-Boltzmann Cell Model for Heterogeneously Charged Colloids. *PRE* **2009**, *80*, 041402.
(33) Anderson, J. A.; Lorenz, C. D.; Travesset, A. General Purpose Molecular Dynamics Simulations Fully Implemented on Graphics Processing Units. *J. Comput. Phys.* **2008**, *227*, 5342−5359.
(34) Glaser, J.; Nguyen, T. D.; Anderson, J. A.; Lui, P.; Spiga, F.; Millan, J. A.; Morse, D. C.; Glotzer, S. C. Strong Scaling of General-Purpose Molecular Dynamics Simulations on GPUs. *Comput. Phys. Commun.* **2015**, *192*, 97−107.
(35) Nguyen, T. D.; Phillips, C. L.; Anderson, J. A.; Glotzer, S. C. Rigid Body Constraints Realized in Massively Parallel Molecular Dynamics on Graphics Processing Units. *Comput. Phys. Commun.* **2011**, *182*, 2307−2313.
(36) More information and the source code for HOOMD-Blue can be found at http://codeblue.umich.edu/hoomd-blue (Accessed June 2, 2016).

DOI: 10.1021/acsnano.6b01218
ACS Nano 2016, 10, 5909−5915